



Article

Off-Grid DoA Estimation on Non-Uniform Linear Array Using Constrained Hermitian Matrix

Hyeonjin Chung ¹, Jeungmin Joo ² and Sunwoo Kim ^{1,*}

¹ Department of Electronics and Computer Engineering, Hanyang University, Seoul 04763, Korea; hyeonjingo@hanyang.ac.kr

² Yuseong P.O. Box 35, Agency for Defense Development, Daejeon 34186, Korea; gangsang@add.re.kr

* Correspondence: remero@hanyang.ac.kr

Received: 22 September 2020; Accepted: 3 November 2020; Published: 4 November 2020



Abstract: In this paper, an off-grid direction-of-arrival (DoA) estimation algorithm which can work on a non-uniform linear array (NULA) is proposed. The original semidefinite programming (SDP) representation of the atomic norm exploits a summation of one-rank matrices constructed by atoms, where the summation of one-rank matrices equals a Hermitian Toeplitz matrix when using the uniform linear array (ULA). On the other hand, when the antennas in the array are placed arbitrarily, the summation of one-rank matrices is a Hermitian matrix whose diagonal elements are equivalent. Motivated by this property, the proposed algorithm replaces the Hermitian Toeplitz matrix in the original SDP with the constrained Hermitian matrix. Additionally, when the antennas are placed symmetrically, the performance can be enforced by adding extra constraints to the Hermitian matrix. The simulation results show that the proposed algorithm achieves higher estimation accuracy and resolution than other algorithms on both array structures; i.e., the arbitrary array and the symmetric array.

Keywords: non-uniform linear array (NULA); off-grid direction-of-arrival (DoA) estimation; atomic norm minimization (ANM); continuous compressive sensing; super-resolution

1. Introduction

Direction-of-arrival (DoA) estimation is one of the longest-studied research topics in array signal processing. DoA estimation algorithms have been adopted in various applications, such as source localization [1] and time-reversal imaging [2,3]. For the localization of target signal sources, distributed sensor arrays estimate the DoAs of target signal sources and then find the location of signal sources using a triangulation method [4]. In the case of time-reversal imaging, the transmitting source generates the probing fields, and the receiving array measures the field scattered by the target object. An image of scattering points can be retrieved by TR-MUSIC [2,3], where TR-MUSIC is derived from MUSIC [5], one of the well-known DoA estimation algorithms. The localization of vehicles in a global positioning system (GPS)-outage scenario has been recently studied in [6–9], and the DoA information is expected to be employed for accurate localization. In a vehicular network context, the position, relative distance and DoAs of neighboring vehicles can be shared via inter-vehicle communication. Using the aforementioned information, the position of vehicles that are out of GPS range can be estimated using cooperative localization [7–9]. As the commercialization of an automotive multiple-input–multiple-output (MIMO) radar progresses [10], it is possible for vehicles to harness the DoAs of other vehicles using the DoA estimation algorithm.

Traditional DoA estimation algorithms such as MUSIC [5] and ESPRIT [11] have high estimation accuracy and resolution. However, they require a large number of snapshots to estimate a covariance matrix and cannot properly estimate the DoAs of coherent signal sources [12] unless they employ

an additional technique such as a spatial smoothing [13]. To overcome the disadvantages of [5,11], another approach for DoA estimation has been proposed in [12,14,15], where the authors exploit various types of compressive sensing (CS) techniques including basis pursuit (BP) [16] and orthogonal matching pursuit (OMP). Normally, CS-based DoA estimation algorithms can successfully estimate DoAs by using a small number of snapshots [17]. CS-based DoA estimation exploits a discretized search grid that consists of angular bases; however, there is a high possibility that the DoAs do not correspond perfectly with the angular bases. The mismatch between the DoAs and the angular bases is generally referred to as a grid-mismatch and induces an estimation error [18]. The grid-mismatch can be alleviated by using a finer search grid. However, using a finer search grid increases the computational complexity, where the complexity of CS is proportional to the grid size [19].

A new approach of exploiting atomic norm minimization (ANM) for DoA estimation has been studied; the mathematical definition of the atomic norm is proposed in [20]. This new approach is often referred to as off-grid DoA estimation and was first proposed in [21], where the new approach based on ANM eliminates the grid-mismatch by working directly on the continuous angular domain. Studies in [22] provide criteria for determining a regularization parameter that helps to retrieve DoAs from a noisy signal. Recently, off-grid azimuth and elevation estimation were proposed in [23], and its application to multiple-input–multiple-output (MIMO) radar is discussed in [24]. However, existing studies regarding off-grid DoA estimation are limited to a uniform linear array (ULA). Since the semidefinite programming (SDP) representation for the atomic norm changes with the array structure, the original SDP representation in former studies does not work under the non-uniform linear array (NULA). Recently, off-grid algorithms that can work on arbitrary array geometries were proposed in [25,26]. However, the placement of the arbitrary array used in [25] is not completely random. Rather, the spacing of adjacent antennas must be a multiple of the preset minimum unit spacing. The algorithm in [26] was motivated by the work presented in [27], where the algorithm enables the usage of an arbitrary array by exploiting the truncated Fourier series-based approximation in [27].

In this paper, we propose a novel approach for off-grid DoA estimation which can work on an NULA. When using an NULA whose antennas are arbitrarily placed, a Hermitian Toeplitz matrix in the SDP targeted for the ULA is replaced by a Hermitian matrix whose diagonal elements are equivalent. Furthermore, when antennas are symmetrically placed, the DoA estimation performance can be improved by adding extra constraints to the Hermitian matrix. The main contributions of this paper are as follows:

- Most of the existing works regarding off-grid DoA estimation are limited to ULA. To overcome this disadvantage, we propose a novel approach for an off-grid DoA estimation algorithm which can work on the NULA. The derivation of the SDP targeted for ULA exploits the property that a summation of the one-rank matrices is equivalent to the Hermitian Toeplitz matrix, where the one-rank matrix is an outer product of identical array manifold vectors. When using the NULA, the summation of the one-rank matrices corresponds to the constrained Hermitian matrix whose diagonal elements are equal. Motivated by this property, we enable the usage of the NULA by replacing the Hermitian Toeplitz matrix with the constrained Hermitian matrix.
- Although the antenna placement of the NULA can be completely arbitrary, it is also possible for antennas to be placed symmetrically with respect to the center. In the case of using the symmetric array, we propose an algorithm for a symmetric array which can enhance the estimation accuracy. When antennas of the NULA are symmetrically placed, the summation of the one-rank matrices corresponds to a unique Hermitian matrix whose particular elements are equal in a certain manner. We model this unique Hermitian matrix by adding extra constraints to the SDP.

Table 1 provides a list of the main symbols used in the paper, and the rest of this paper is organized as follows. Section 2 presents the received signal model. Section 3 describes the proposed off-grid DoA estimation algorithm for the NULA. Simulation results are provided in Section 4, and finally Section 5 gives concluding remarks.

Table 1. List of main symbols used in this paper. DoA: direction of arrival.

Symbol	Description	Symbol	Description
P	Number of DoAs	M	Number of antennas
λ	Wavelength of signal	d_m	Distance between the m -th antenna and the reference
θ_p	DoA of the p -th signal source	Θ	Vector consists of P DoAs
$\mathbf{a}(\theta)$	Steering vector whose DoA is θ	\mathbf{x}	Received signal
\mathbf{s}	Signal from P signal sources	σ_s^2	Power of signal

We use lower-case and upper-case bold characters to represent vectors and matrices, respectively, throughout this paper. $(\cdot)^T$, $(\cdot)^H$ and $(\cdot)^*$, respectively, denote transpose, conjugate transpose and complex conjugation. $\text{Trace}(\cdot)$ denotes the trace of a matrix. The curled inequality symbol \succeq denotes matrix inequality. If $\mathbf{A} \succeq \mathbf{B}$, a matrix $\mathbf{A} - \mathbf{B}$ is positive semidefinite. $\mathbf{a}(i)$ denotes the i -th element in a vector \mathbf{a} , and $\mathbf{A}(i, j)$ denotes the (i, j) -th element in a matrix \mathbf{A} . $\mathbf{0}_N$ denotes a $N \times 1$ zero vector, and \mathbf{I}_N denotes a $N \times N$ identity matrix. $\lfloor \cdot \rfloor$ denotes rounding down.

2. Signal Model

We consider P narrowband signals impinging on the antenna array, where the antenna array is composed of M antennas. f denotes the carrier frequency of the signal. The DoAs of P signal sources are denoted as $\Theta = (\theta_1, \dots, \theta_P)^T$. An array manifold vector whose DoA is θ , $\mathbf{a}(\theta)$ can be given as

$$\mathbf{a}(\theta) = \left(e^{j2\pi(d_1/\lambda)\cos\theta}, \dots, e^{j2\pi(d_M/\lambda)\cos\theta} \right)^T \in \mathbb{C}^{M \times 1}, \quad (1)$$

where d_m denotes the distance between the m -th antenna and the reference antenna, and $\lambda = c/f$. Note that c is the speed of light. $\mathbb{C}^{M \times 1}$ denotes a complex vector with the size of $M \times 1$, and this notation can also represent the complex matrix. The first antenna is the reference antenna, if not noted, and thus $d_1 = 0$. An array manifold matrix for P signal sources, $\mathbf{A}(\Theta)$, is

$$\mathbf{A}(\Theta) = (\mathbf{a}(\theta_1), \dots, \mathbf{a}(\theta_P)) \in \mathbb{C}^{M \times P}. \quad (2)$$

The received signal \mathbf{x} can be given by

$$\mathbf{x} = \mathbf{A}(\Theta)\mathbf{s} \in \mathbb{C}^{M \times 1}. \quad (3)$$

$\mathbf{s} = (s_1, \dots, s_P)^T$, where s_p denotes the single signal snapshot from the p -th signal source. \mathbf{s} follows $\mathcal{CN}(\mathbf{0}_P, \sigma_s^2 \mathbf{I}_P)$, where σ_s^2 denotes the power of the signal, and $\mathcal{CN}(\mathbf{0}_P, \sigma_s^2 \mathbf{I}_P)$ represents a circularly symmetric Gaussian random vector whose mean is $\mathbf{0}_P$ and covariance is $\sigma_s^2 \mathbf{I}_P$.

3. Off-Grid DoA Estimation Algorithm on Non-Uniform Linear Array Using Constrained Hermitian Matrix

In this section, the off-grid DoA estimation algorithms for the arbitrary array and the symmetric array are explained. Examples of the ULA, the arbitrary array and the symmetric array are given in Figure 1. Note that the spacing between adjacent antennas in the arbitrary array is completely random. On the other hand, the antennas in the symmetric array are placed symmetrically with respect to the center of the array, with the spacing between adjacent antennas being random.

3.1. Arbitrary Linear Array Case

The atomic norm of \mathbf{x} can be given by

$$\begin{aligned} \|\mathbf{x}\|_{\mathcal{A}} &= \inf \{g > 0 : \mathbf{x} \in g \text{conv}(\mathcal{A})\} \\ &= \inf \left\{ \sum_{l=1}^L |h_l| \mid \mathbf{x} = \sum_{l=1}^L h_l \mathbf{a}(\theta_l) \right\}, \end{aligned} \quad (4)$$

where $\text{conv}(\cdot)$ denotes a convex hull of a given set, \mathcal{A} is an atomic set, g is an arbitrary positive number that satisfies $\mathbf{x} \in g\text{conv}(\mathcal{A})$, and L is the number of atoms that forms \mathbf{x} . $\mathbf{a}(\vartheta_l)$ is the l -th atom, and $\mathcal{A} = \{\mathbf{a}(\vartheta) \mid 0^\circ < \vartheta < 180^\circ\}$. h_l is a coefficient of the l -th atom which satisfies $\mathbf{x} = \sum_{l=1}^L h_l \mathbf{a}(\vartheta_l)$ for arbitrary $\{\vartheta_l\}$, where $\{\vartheta_l\}$ denotes ϑ_l for $l = 1, \dots, L$. The details of the convex hull and its relationship with the atomic norm are well-explained in the seminal works of the atomic norm [20,21,28]. When using the ULA, the SDP representation of $\|\mathbf{x}\|_{\mathcal{A}}$ can be given by follows, as in [28].

$$\begin{aligned} \|\mathbf{x}\|_{\mathcal{A}} = \min_{\mathbf{u}, t} & \left\{ \frac{1}{2M} \text{Trace}(\text{Toep}(\mathbf{u})) + \frac{1}{2}t \right\} \\ \text{s.t.} & \begin{bmatrix} \text{Toep}(\mathbf{u}) & \mathbf{x} \\ \mathbf{x}^H & t \end{bmatrix} \succeq 0, t \geq 0. \end{aligned} \tag{5}$$

$\text{Toep}(\mathbf{u})$ —a Hermitian Toeplitz matrix whose first column is \mathbf{u} —can be denoted as

$$\text{Toep}(\mathbf{u}) = \begin{bmatrix} \mathbf{u}(1) & \mathbf{u}^*(2) & \dots & \mathbf{u}^*(M) \\ \mathbf{u}(2) & \mathbf{u}(1) & \dots & \mathbf{u}^*(M-1) \\ \vdots & \vdots & \ddots & \vdots \\ \mathbf{u}(M) & \mathbf{u}(M-1) & \dots & \mathbf{u}(1) \end{bmatrix}. \tag{6}$$

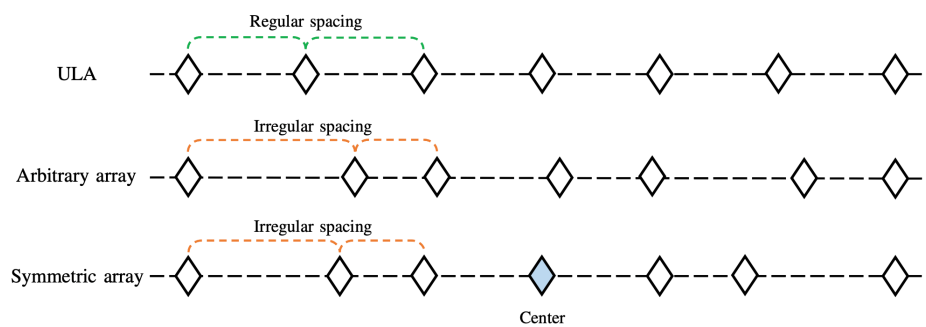


Figure 1. Examples of a uniform linear array (ULA), arbitrary array and symmetric array. The blue antenna denotes the center of the symmetric array.

However, when antennas are placed arbitrarily so that the spacing between adjacent antennas is non-uniform, the SDP representation in (5) can no longer be used. In this case, the SDP formulation in (5) can be modified as follows:

$$\begin{aligned} \min_{\mathbf{H}, t} & \left\{ \frac{1}{2M} \text{Trace}(\mathbf{H}) + \frac{1}{2}t \right\} \\ \text{s.t.} & \begin{bmatrix} \mathbf{H} & \mathbf{x} \\ \mathbf{x}^H & t \end{bmatrix} \succeq 0, t \geq 0, \end{aligned} \tag{7}$$

\mathbf{H} is a Hermitian matrix,
 $\mathbf{H}(1,1) = \mathbf{H}(2,2) \dots = \mathbf{H}(M,M)$.

In Figure 2, the example of $\text{Toep}(\mathbf{u})$ for the ULA and \mathbf{H} for the arbitrary array is given, and the relationship between elements is displayed. To show that diagonal elements of \mathbf{H} are equal, we define \mathbf{B}_i for $i = 1, \dots, M - 1$ as follows.

$$\begin{aligned} \mathbf{B}_i(1,1) &= 1, \\ \mathbf{B}_i(i+1, i+1) &= -1, \text{ for } i = 1, \dots, M - 1. \end{aligned} \tag{8}$$

Using \mathbf{B}_i for $i = 1, \dots, M - 1$, (7) can be reformulated as

$$\begin{aligned} \min_{\mathbf{H}, t} & \left\{ \frac{1}{2M} \text{Trace}(\mathbf{H}) + \frac{1}{2}t \right\} \\ \text{s.t.} & \begin{bmatrix} \mathbf{H} & \mathbf{x} \\ \mathbf{x}^H & t \end{bmatrix} \succeq 0, t \geq 0, \\ & \mathbf{H} \text{ is a Hermitian matrix,} \\ & \text{Trace}(\mathbf{B}_i \mathbf{H}) = 0, \text{ for } i = 1, \dots, M - 1. \end{aligned} \tag{9}$$

After solving (9), MUSIC [5] is applied to obtain the spatial spectrum and estimate DoAs. Note that the approach of applying MUSIC after solving the SDP has been employed in the seminal works of off-grid DoA estimation [29–31]. Letting $\hat{\mathbf{H}}$ denote the optimal solution of \mathbf{H} , $\hat{\mathbf{H}}$ is considered as the covariance matrix in MUSIC and is decomposed into a set of eigenvectors and eigenvalues as follows:

$$\hat{\mathbf{H}} = \mathbf{Q}_H \mathbf{\Sigma}_H \mathbf{Q}_H^H, \tag{10}$$

where \mathbf{Q}_H is a matrix that is composed of eigenvectors of $\hat{\mathbf{H}}$, and $\mathbf{\Sigma}_H$ is a diagonal matrix whose diagonal elements are eigenvalues of $\hat{\mathbf{H}}$. Eigenvalues are sorted such that $\mathbf{\Sigma}_H(1, 1) > \mathbf{\Sigma}_H(2, 2) \dots > \mathbf{\Sigma}_H(M, M)$. The DoAs can be estimated by finding P largest peaks from the spatial spectrum $f_H(\theta)$, which is

$$f_H(\theta) = \frac{1}{\mathbf{a}(\theta)^H \mathbf{Q}_H(P+1:M) \mathbf{Q}_H(P+1:M)^H \mathbf{a}(\theta)}, \tag{11}$$

for $0^\circ < \theta < 180^\circ$,

where $\mathbf{Q}_H(P+1:M)$ denotes a matrix that is composed of consecutive columns from the $(P+1)$ -th column of \mathbf{Q}_H to the M -th column.

⟨ULA⟩ Toep(u) ∈ ℂ ^{M×M}				⟨Arbitrary array⟩ H ∈ ℂ ^{M×M}				⟨Symmetric array⟩ G ∈ ℂ ^{M×M}			
u(1)	u*(2)	u*(3)	u*(4)	H(1,1)	H(1,2)	H(1,3)	H(1,4)	G(1,1)	G(1,2)	G(1,3)	G(1,4)
u(2)	u(1)	u*(2)	u*(3)	H(2,1)	H(2,2)	H(2,3)	H(2,4)	G(2,1)	G(2,2)	G(2,3)	G(2,4)
u(3)	u(2)	u(1)	u*(2)	H(3,1)	H(3,2)	H(3,3)	H(3,4)	G(3,1)	G(3,2)	G(3,3)	G(3,4)
u(4)	u(3)	u(2)	u(1)	H(4,1)	H(4,2)	H(4,3)	H(4,4)	G(4,1)	G(4,2)	G(4,3)	G(4,4)

Figure 2. Elements of the Hermitian Toeplitz matrix, constrained matrix for arbitrary array \mathbf{H} and constrained matrix for symmetric array \mathbf{G} . Here, $M = 4$. Note that colors are used to display which elements are equal. Since all matrices are Hermitian matrices, the upper sides of the matrices are not colored.

Remark 1. The SDP representation of $\|\mathbf{x}\|_{\mathcal{A}}$ can be derived by using a linear matrix inequality. Here, note that $\mathbf{x} = \sum_{p=1}^P s_p \mathbf{a}(\theta_p)$. The linear matrix inequality that is employed for the SDP representation of $\|\mathbf{x}\|_{\mathcal{A}}$ can be given by

$$t \sum_{l=1}^L d_l \mathbf{a}(\vartheta_l) \mathbf{a}(\vartheta_l)^H - \mathbf{x} \mathbf{x}^H \succeq 0, t \geq 0, d_l > 0, \text{ for } l = 1, \dots, L. \tag{12}$$

Suppose $t/2 + \sum_{l=1}^L d_l$ is minimized while t , $\{d_l\}$, and $\{\vartheta_l\}$ satisfy (12); then, $L = P$ and $t = \sum_{p=1}^P |s_p|$ [21]. Additionally, $\vartheta_p = \theta_p$ and $d_p = |s_p|$ for $p = 1, \dots, P$. Note that when the ULA is

employed, the summation of one-rank matrices $\sum_{l=1}^L d_l \mathbf{a}(\vartheta_l) \mathbf{a}(\vartheta_l)^H$ is a Hermitian Toeplitz matrix. According to the Vandermonde decomposition theorem [30], it is also possible to represent the Hermitian Toeplitz matrix as $\sum_{l=1}^L d_l \mathbf{a}(\vartheta_l) \mathbf{a}(\vartheta_l)^H$. When replacing $\sum_{l=1}^L d_l \mathbf{a}(\vartheta_l) \mathbf{a}(\vartheta_l)^H$ with the Hermitian Toeplitz matrix $\text{Toep}(\mathbf{u})$, Equation (12) can be rewritten as

$$t \text{Toep}(\mathbf{u}) - \mathbf{x} \mathbf{x}^H \succeq 0, t \geq 0. \quad (13)$$

By using the Schur complement, (13) can be represented as

$$\begin{bmatrix} \text{Toep}(\mathbf{u}) & \mathbf{x} \\ \mathbf{x}^H & t \end{bmatrix} \succeq 0, t \geq 0, \quad (14)$$

where (14) is equivalent to the constraint of (5). However, when using the NULA, $\sum_{l=1}^L d_l \mathbf{a}(\vartheta_l) \mathbf{a}(\vartheta_l)^H$ is no longer the Hermitian Toeplitz matrix, but a Hermitian matrix whose diagonal elements are equal. Thus, for the NULA case, we replace the Hermitian Toeplitz matrix in (5) with a constrained Hermitian matrix whose diagonal elements are equal.

3.2. Symmetric Array Case

Although the antenna placement of the NULA can be completely arbitrary, the antennas can be placed in a certain manner; e.g., placing antennas symmetrically. When antennas are placed symmetrically, particular elements of $\sum_{l=1}^L d_l \mathbf{a}(\vartheta_l) \mathbf{a}(\vartheta_l)^H$ are equivalent to each other. Let $\mathbf{G} \in \mathbb{C}^{M \times M}$ denote $\sum_{l=1}^L d_l \mathbf{a}(\vartheta_l) \mathbf{a}(\vartheta_l)^H$ when using the symmetric array; \mathbf{G} has following unique properties:

- \mathbf{G} is a Hermitian matrix.
- All diagonal elements of \mathbf{G} are equal such that $\mathbf{G}(1,1) = \mathbf{G}(2,2) \dots = \mathbf{G}(M,M)$.
- $\mathbf{G}(i+j, j) = \mathbf{G}(M-j+1, M-i-j+1)$ for $i = 1, \dots, M-2j$ and $j = 1, \dots, \lfloor (M-1)/2 \rfloor$.

In Figure 2, the example of \mathbf{G} for the symmetric array is given, and the relationship between elements is displayed. To represent these properties within the constraints of SDP, we define \mathbf{C}_i^j for $i = 1, \dots, M-2j$ and $j = 1, \dots, \lfloor (M-1)/2 \rfloor$ as follows.

$$\begin{aligned} \mathbf{C}_i^j(i+j, j) &= 1, \quad \mathbf{C}_i^j(M-j+1, M-i-j+1) = -1, \\ \text{for } i &= 1, \dots, M-2j, \quad j = 1, \dots, \left\lfloor \frac{M-1}{2} \right\rfloor. \end{aligned} \quad (15)$$

With \mathbf{B}_i and \mathbf{C}_i^j , the SDP formulation for the symmetric array can be given by

$$\begin{aligned} \min_{\mathbf{G}, t} & \left\{ \frac{1}{2M} \text{Trace}(\mathbf{G}) + \frac{1}{2} t \right\} \\ \text{s.t.} & \begin{bmatrix} \mathbf{G} & \mathbf{x} \\ \mathbf{x}^H & t \end{bmatrix} \succeq 0, t \geq 0, \\ & \mathbf{G} \text{ is a Hermitian matrix,} \\ & \text{Trace}(\mathbf{B}_i \mathbf{G}) = 0, \text{ for } i = 1, \dots, M-1, \\ & \text{Trace}(\mathbf{C}_i^j \mathbf{G}) = 0, \\ & \text{for } i = 1, \dots, M-2j, \quad j = 1, \dots, \left\lfloor \frac{M-1}{2} \right\rfloor. \end{aligned} \quad (16)$$

After solving (16), MUSIC is applied to obtain the spatial spectrum and estimate DoAs. Letting $\hat{\mathbf{G}}$ denote the optimal solution of \mathbf{G} , $\hat{\mathbf{G}}$ also undergoes the identical procedure as in (10) and (11). An eigen-decomposition of $\hat{\mathbf{G}}$ can be given by

$$\hat{\mathbf{G}} = \mathbf{Q}_G \mathbf{\Sigma}_G \mathbf{Q}_G^H, \quad (17)$$

where \mathbf{Q}_G is a matrix that is composed of eigenvectors of $\hat{\mathbf{G}}$, and $\mathbf{\Sigma}_G$ is a diagonal matrix whose diagonal elements are eigenvalues of $\hat{\mathbf{G}}$. Eigenvalues are sorted such that $\mathbf{\Sigma}_G(1,1) > \mathbf{\Sigma}_G(2,2) \dots > \mathbf{\Sigma}_G(M,M)$. The DoAs can be estimated by finding P largest peaks from spatial spectrum $f_G(\theta)$ which is

$$f_G(\theta) = \frac{1}{\mathbf{a}(\theta)^H \mathbf{Q}_G(P+1:M) \mathbf{Q}_G(P+1:M)^H \mathbf{a}(\theta)}, \quad (18)$$

for $0^\circ < \theta < 180^\circ$.

4. Simulation Result

The performance of the proposed algorithm, OMP [32], conventional delay-sum beamforming (CBF) and the algorithm in [26] are compared in this section. Since only single snapshots are given in the simulation, algorithms that require plenty number of snapshots such as MUSIC and ESPRIT are excluded from the comparison. For the root mean square error (RMSE) analysis, $M = 8$ and $P = 2$. The spacing between adjacent antennas is randomly set between 0.3λ and 0.7λ . For OMP, the size of grid D is set to 360, and the discrete grid spacing is set to 0.5° . Note that as D increases, the grid becomes finer so that the estimation error induced by the grid-mismatch decreases. However, the computational complexity is proportional to D . For the CBF, the resolution of the spectrum is set to 0.01° , and the size of the spectrum R is 18,000. In this case, the spectrum is sufficiently fine, as if DoAs are estimated from the continuous angle domain. For the algorithm in [26], the number of the discrete Fourier transform (DFT) points K is set to 101, where the estimation accuracy of the algorithm in [26] is proportional to K . The root mean square error (RMSE) is defined as

$$\text{RMSE} = \sqrt{\frac{1}{PQ} \sum_{q=1}^Q \left\{ \sum_{p=1}^P (\hat{\theta}_p^q - \theta_p^q)^2 \right\}}, \quad (19)$$

where Q is the number of Monte Carlo trials for RMSE calculation, and θ_p^q and $\hat{\theta}_p^q$, respectively, denote the real DoA and the estimated DoA of the p -th signal source on the q -th trial. For each iteration, DoAs are chosen randomly between $(30^\circ, 150^\circ)$.

4.1. Simulations for Arbitrary Array

In Figure 3, the spectrums of the proposed algorithm for the arbitrary array, OMP, CBF and the algorithm in [26] are given. The antennas are placed arbitrarily as $(0, 0.7, 1.3, 1.8, 2.1, 2.6, 3.0)\lambda$, and $\sigma_s = 1$. The DoAs are sufficiently separated such that $\Theta = (50^\circ, 90^\circ)^T$. Figure 3 shows that the spectrums of all algorithms have peaks around DoAs. From this result, it can be considered that the estimations of all algorithms are accurate if DoAs are sufficiently separated.

However, if DoAs are closely separated, an algorithm with low resolution may exhibit estimation failure. To compare the resolution of DoA estimation algorithms, we define a distance between two adjacent DoAs τ as $\tau = |(\cos \theta_1 - \cos \theta_2)/2|$, where τ is used as a criterion of resolution in [21,28,33]. Note that τ is proportional to the difference between θ_1 and θ_2 as τ becomes 0 when $\theta_1 = \theta_2$. Figure 4 presents the RMSE result versus τ . Here, $\sigma_s = 1$. Figure 4 shows that the proposed algorithm has superior accuracy over OMP, CBF and the algorithm in [26] at every τ . Especially, the RMSE of the proposed algorithm remains low when τ is small, while the RMSE of the other algorithms is large when τ is small. The RMSE of all algorithms tend to decrease as τ increases. From this result, it can be seen that the proposed algorithm has higher resolution than others since the proposed algorithm can accurately estimate two adjacent DoAs. Additionally, the proposed algorithm has higher estimation accuracy even when DoAs are sufficiently separated.

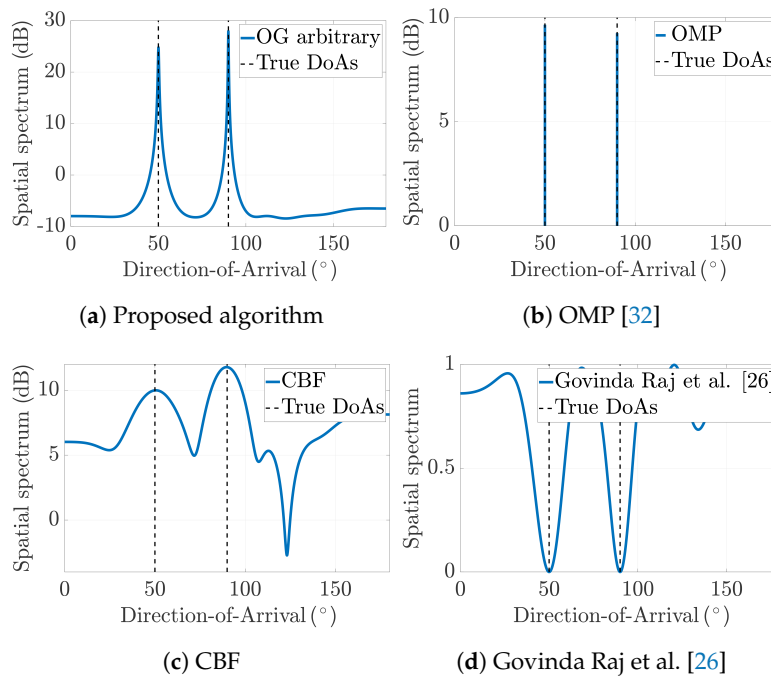


Figure 3. Spectrums of DoA estimation algorithms when using the arbitrary array and $\Theta = [50^\circ, 90^\circ]^T$.

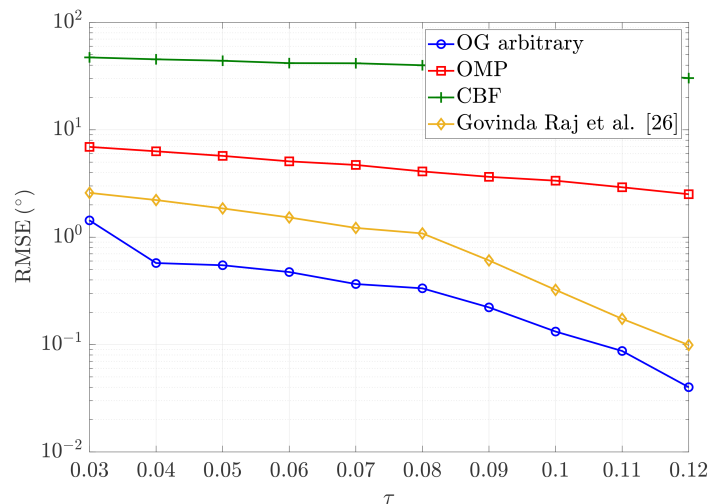


Figure 4. The RMSE of the proposed algorithm, orthogonal matching pursuit (OMP) and conventional delay-sum beamforming (CBF) versus τ . A total of 1000 Monte Carlo trials are conducted.

4.2. Simulations for Symmetric Array

In Figure 5, the spectrums of the algorithm for the symmetric array, the algorithm for the arbitrary array, OMP, CBF and the algorithm in [26] are given. The antennas are placed symmetrically as $(0, 0.4, 0.8, 1.5, 2.2, 2.6, 3.0)\lambda$. The DoAs are sufficiently separated such that $\Theta = (50^\circ, 90^\circ)^T$ and $\sigma_s = 1$. Figure 5 shows that the estimation of all algorithms is accurate when DoAs are sufficiently separated. Nevertheless, the spectrum of the algorithm for the symmetric array shows distinct peaks at DoAs while the spectrum of the algorithm for the arbitrary array has dispersed peaks.

For the RMSE analysis, the symmetric array with irregular antenna spacing is used, where the spacing between adjacent antennas is randomly set between 0.3λ and 0.7λ . Figure 6 presents the RMSE result versus τ . Here, $\sigma_s = 1$. In Figure 6, the RMSE of the proposed algorithms for the symmetric array and the arbitrary array are lower than other algorithms at every τ . The RMSE of the proposed algorithms for the symmetric array and the arbitrary array remain low when τ is small, while the RMSE of the other algorithms is large when τ is small. The RMSE of all algorithms tend to decrease

as τ increases. The RMSE of all algorithms tends to decrease as τ increases. From this result, we can conclude that the resolution of the algorithm for the symmetric array is higher than other traditional algorithms, and the algorithm for the symmetric array has a slight superiority over the algorithm for the arbitrary array. Additionally, the algorithm for the symmetric array has higher estimation accuracy when DoAs are sufficiently separated. Thus, the algorithm for the symmetric array is the best option when the symmetric array is employed.

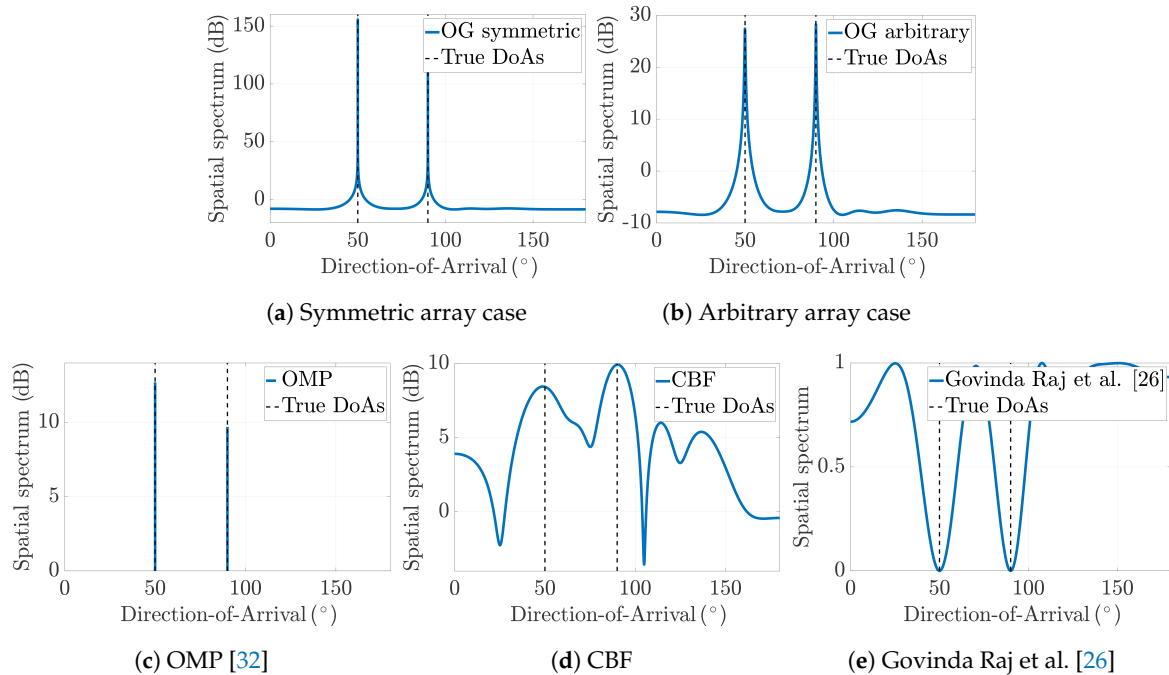


Figure 5. Spectrums of DoA estimation algorithms when using the symmetric array and $\Theta = [50^\circ, 90^\circ]^T$.

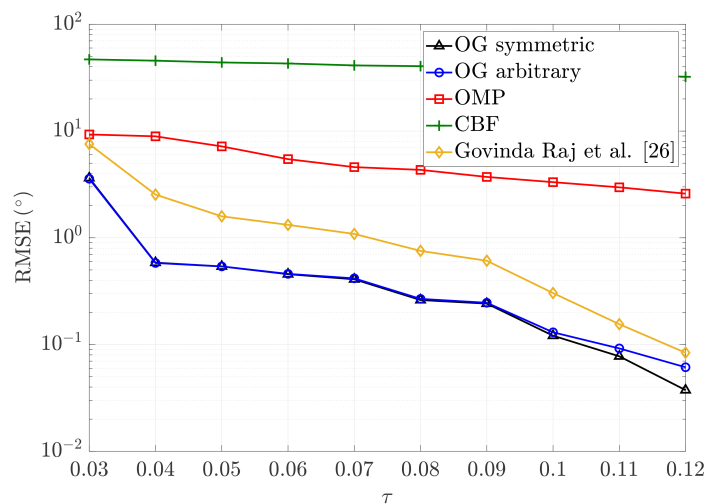


Figure 6. The RMSE of the proposed algorithm for the symmetric array, the proposed algorithm for the arbitrary array, OMP, CBF and the algorithm in [26] versus τ . A total of 1000 Monte Carlo trials are conducted.

4.3. Complexity Analysis

The complexity and the average computation time of DoA estimation algorithms are given in Table 2. For computation, an Intel CPU i5-7500 (3.40 GHz) and 16 GB RAM are used. The complexity of the proposed algorithm for the symmetric array, the proposed algorithm for the arbitrary array and

the algorithm in [26] can be calculated using the analysis in [34], where the complexity of the SDP is derived as in [34]. The complexity of the OMP is taken from [35]. The complexities of the proposed algorithms for both types of NULA and the algorithm in [26] are much higher than OMP and CBF. Among both proposed algorithms, the complexity of the proposed algorithm for the symmetric array is higher than that of the proposed algorithm for the arbitrary array since extra constraints are added to the algorithm for the symmetric array. Although the average computation times of the proposed algorithms are below 1 s, the computation time of the proposed algorithms may surge as the number of antennas increases. When using the algorithm in [26], K must be much bigger than M for accurate estimation. Thus, the average computation time of the algorithm in [26] is larger than other algorithms.

Table 2. The complexity and average computation time of DoA estimation algorithms.

Algorithm	Complexity	Computation Time
Proposed algorithm for the symmetric array	$O(M^2(M+1)^{3.5})$	0.33 s
Proposed algorithm for the arbitrary array	$O(M(M+1)^{3.5})$	0.28 s
OMP [32]	$O(PMD)$	0.0068 s
CBF	$O(MR)$	0.078 s
Govinda Raj et al. [26]	$O(K(K+1)^{3.5})$	3.08 s

5. Conclusions

In this paper, we propose a novel off-grid DoA estimation algorithm which can work on two types of NULA; i.e., an arbitrary array and a symmetric array. The proposed algorithm is motivated by the original SDP representation in former studies that only work on the ULA. In the derivation of the original SDP, the received signal and the summation of one-rank matrices constructed by atoms are exploited, where the summation of one-rank matrices equals the Hermitian Toeplitz matrix when using the ULA. On the other hand, when using the NULA, the summation of one-rank matrices is no longer the Hermitian Toeplitz matrix but rather the Hermitian matrix, whose diagonal elements are equal. Besides, when the antennas in the NULA are placed symmetrically, extra constraints can be added to the summation of one-rank matrices. Thus, the proposed algorithm replaces the Hermitian Toeplitz matrix in the original SDP with the constrained Hermitian matrix, where the constraints vary with the array structure. Simulation results present the superiority of the proposed algorithm, especially in terms of estimation accuracy and resolution, compared to other algorithms on both array structures; i.e., the arbitrary array and the symmetric array. The proposed algorithm can be extended to practical applications such as localization in vehicular networks and automotive radar. However, the complexity analysis shows that the computation time of the proposed algorithm may no longer be negligible when the number of antennas increases. Thus, a method to reduce the complexity of the proposed algorithm needs to be studied for the broader application of the proposed algorithm.

Author Contributions: Conceptualization, H.C.; Methodology, H.C.; Software, H.C.; Validation, H.C. and S.K.; Formal analysis, H.C.; Investigation, H.C.; Resources, H.C., J.J. and S.K.; Data curation, H.C.; Writing—original draft preparation, H.C. and S.K.; Visualization, H.C.; Supervision, S.K.; Project administration, J.J. and S.K.; Funding acquisition, S.K. All authors have read and agreed to the published version of the manuscript.

Funding: This research received no external funding.

Acknowledgments: This work was supported by the Agency for Defense Development.

Conflicts of Interest: The authors declare no conflict of interest.

References

1. Chen, J.C.; Kung Yao.; Hudson, R.E. Source localization and beamforming. *IEEE Signal Process. Mag.* **2002**, *19*, 30–39.
2. Marengo, E.A.; Gruber, F.K.; Simonetti, F. Time-Reversal MUSIC Imaging of Extended Targets. *IEEE Trans. Image Process.* **2007**, *16*, 1967–1984. [[PubMed](#)]

3. Ciunozzo, D.; Romano, G.; Solimene, R. Performance Analysis of Time-Reversal MUSIC. *IEEE Trans. Signal Process.* **2015**, *63*, 2650–2662.
4. Liu, H.; Darabi, H.; Banerjee, P.; Liu, J. Survey of Wireless Indoor Positioning Techniques and Systems. *IEEE Trans. Syst. Man Cybern. Part C (Appl. Rev.)* **2007**, *37*, 1067–1080.
5. Schmidt, R. Multiple emitter location and signal parameter estimation. *IEEE Trans. Ant. Propag.* **1986**, *34*, 276–280. [[CrossRef](#)]
6. Kaiwartya, O. Geometry-Based Localization for GPS Outage in Vehicular Cyber Physical Systems. *IEEE Trans. Veh. Technol.* **2018**, *67*, 3800–3812.
7. Hassan, A.N. Geometry Based Inter Vehicle Distance Estimation for Instantaneous GPS Failure in VANETs. In Proceedings of the Second International Conference on Information and Communication Technology for Competitive Strategies, Austin, TX, USA, 4–5 March 2016. [[CrossRef](#)]
8. Wymeersch, H.; Seco-Granados, G.; Destino, G.; Dardari, D.; Tufvesson, F. 5G mmWave Positioning for Vehicular Networks. *IEEE Wirel. Commun.* **2017**, *24*, 80–86.
9. Eom, J.; Kim, H.; Lee, S.H.; Kim, S. DNN-Assisted Cooperative Localization in Vehicular Networks. *Energies* **2019**, *12*, 2758. [[CrossRef](#)]
10. Hasch, J.; Topak, E.; Schnabel, R.; Zwick, T.; Weigel, R.; Waldschmidt, C. Millimeter-Wave Technology for Automotive Radar Sensors in the 77 GHz Frequency Band. *IEEE Trans. Microw. Theory Tech.* **2012**, *60*, 845–860.
11. Roy, R.; Kailath, T. ESPRIT-estimation of signal parameters via rotational invariance techniques. *IEEE Trans. Acoust. Speech Signal Process.* **1989**, *37*, 984–995.
12. Malioutov, D.; Cetin, M.; Willsky, A.S. A sparse signal reconstruction perspective for source localization with sensor arrays. *IEEE Trans. Signal Process.* **2005**, *53*, 3010–3022. [[CrossRef](#)]
13. Shan, T.J.; Wax, M.; Kailath, T. On spatial smoothing for direction-of-arrival estimation of coherent signals. *IEEE Trans. Acoust. Speech Signal Process.* **1985**, *33*, 806–811. [[CrossRef](#)]
14. Gorodnitsky, I.F.; Rao, B.D. Sparse signal reconstruction from limited data using FOCUSS: A re-weighted minimum norm algorithm. *IEEE Trans. Signal Process.* **1997**, *45*, 600–616.
15. Yang, Z.; Xie, L.; Zhang, C. Off-Grid Direction of Arrival Estimation Using Sparse Bayesian Inference. *IEEE Trans. Signal Process.* **2013**, *61*, 38–43. [[CrossRef](#)]
16. Chen, S.S.; Donoho, D.L.; Saunders, M.A. Atomic decomposition by Basis Pursuit. *SIAM J. Sci. Comput.* **1999**, *20*, 33–61.
17. Shen, Q.; Liu, W.; Cui, W.; Wu, S. Underdetermined DOA Estimation Under the Compressive Sensing Framework: A Review. *IEEE Access* **2016**, *4*, 8865–8878. [[CrossRef](#)]
18. Chi, Y.; Scharf, L.L.; Pezeshki, A.; Calderbank, A.R. Sensitivity to Basis Mismatch in Compressed Sensing. *IEEE Trans. Signal Process.* **2011**, *59*, 2182–2195. [[CrossRef](#)]
19. Baraniuk, R.G. Compressive Sensing [Lecture Notes]. *IEEE Signal Process. Mag.* **2007**, *24*, 118–121. [[CrossRef](#)]
20. Chandrasekaran, V.; Recht, B.; Parrilo, P.A.; Willsky, A.S. The Convex Geometry of Linear Inverse Problems. *Found. Comput. Math.* **2012**, *12*, 805–849. [[CrossRef](#)]
21. Tang, G.; Bhaskar, B.N.; Shah, P.; Recht, B. Compressed Sensing Off the Grid. *IEEE Trans. Inf. Theory* **2013**, *59*, 7465–7490. [[CrossRef](#)]
22. Bhaskar, B.N.; Tang, G.; Recht, B. Atomic Norm Denoising with Applications to Line Spectral Estimation. *IEEE Trans. Signal Process.* **2013**, *61*, 5987–5999. [[CrossRef](#)]
23. Tian, Z.; Zhang, Z.; Wang, Y. Low-complexity optimization for two-dimensional direction-of-arrival estimation via decoupled atomic norm minimization. In Proceedings of the 2017 IEEE International Conference on Acoustics, Speech and Signal Processing (ICASSP), New Orleans, LA, USA, 5–9 March 2017; pp. 3071–3075.
24. Tang, W.; Jiang, H.; Pang, S. Grid-Free DOD and DOA Estimation for MIMO Radar via Duality-Based 2D Atomic Norm Minimization. *IEEE Access* **2019**, *7*, 60827–60836. [[CrossRef](#)]
25. Sanchez-Fernandez, M.; Jamali, V.; Llorca, J.; Tulino, A. Gridless Multidimensional Angle of Arrival Estimation for Arbitrary 3D Antenna Arrays. *arXiv* **2020**, arXiv:cs.IT/2008.12323.
26. Govinda Raj, A.; McClellan, J.H. Single Snapshot Super-Resolution DOA Estimation for Arbitrary Array Geometries. *IEEE Signal Process. Lett.* **2019**, *26*, 119–123. [[CrossRef](#)]

27. Rubsamen, M.; Gershman, A.B. Direction-of-Arrival Estimation for Nonuniform Sensor Arrays: From Manifold Separation to Fourier Domain MUSIC Methods. *IEEE Trans. Signal Process.* **2009**, *57*, 588–599. [[CrossRef](#)]
28. Chi, Y.; Ferreira Da Costa, M. Harnessing Sparsity Over the Continuum: Atomic norm minimization for superresolution. *IEEE Signal Process. Mag.* **2020**, *37*, 39–57. [[CrossRef](#)]
29. Zhou, C.; Gu, Y.; Fan, X.; Shi, Z.; Mao, G.; Zhang, Y.D. Direction-of-Arrival Estimation for Coprime Array via Virtual Array Interpolation. *IEEE Trans. Signal Process.* **2018**, *66*, 5956–5971. [[CrossRef](#)]
30. Yang, Z.; Xie, L.; Stoica, P. Vandermonde Decomposition of Multilevel Toeplitz Matrices With Application to Multidimensional Super-Resolution. *IEEE Trans. Inf. Theory* **2016**, *62*, 3685–3701. [[CrossRef](#)]
31. Li, Y.; Chi, Y. Off-the-Grid Line Spectrum Denoising and Estimation With Multiple Measurement Vectors. *IEEE Trans. Signal Process.* **2016**, *64*, 1257–1269. [[CrossRef](#)]
32. Cai, T.T.; Wang, L. Orthogonal Matching Pursuit for Sparse Signal Recovery With Noise. *IEEE Trans. Inf. Theory* **2011**, *57*, 4680–4688. [[CrossRef](#)]
33. Candès, E.; Fernandez-Granda, C. Towards a Mathematical Theory of Super-Resolution. *Commun. Pure Appl. Math.* **2014**, *67*, 906–956. [[CrossRef](#)]
34. Pólik, I.; Terlaky, T. Interior Point Methods for Nonlinear Optimization. In *Nonlinear Optimization*; Di Pillo, G., Schoen, F., Eds.; Springer: Berlin/Heidelberg, Germany, 2010; pp. 215–276. [[CrossRef](#)]
35. Wang, J.; Kwon, S.; Shim, B. Generalized Orthogonal Matching Pursuit. *IEEE Trans. Signal Process.* **2012**, *60*, 6202–6216. [[CrossRef](#)]

Publisher’s Note: MDPI stays neutral with regard to jurisdictional claims in published maps and institutional affiliations.



© 2020 by the authors. Licensee MDPI, Basel, Switzerland. This article is an open access article distributed under the terms and conditions of the Creative Commons Attribution (CC BY) license (<http://creativecommons.org/licenses/by/4.0/>).